Monthly Notices
of the
ROYAL ASTRONOMICAL SOCIETY

MNRAS **493,** 2339–2351 (2020)
Advance Access publication 2020 February 17

doi:10.1093/mnras/staa454

Internal motions in OB associations with *Gaia* DR2

A. M. Melnik★ and A. K. Dambis

Sternberg Astronomical Institute, Lomonosov Moscow State University, Universitetskii pr. 13, Moscow, 119991 Russia

Accepted 2020 February 11. Received 2020 January 17; in original form 2019 June 6

ABSTRACT

We study the motions inside 28 OB associations with the use of *Gaia* DR2 proper motions. The average velocity dispersion calculated for 28 OB associations including more than 20 stars with *Gaia* DR2 proper motion is $\sigma_v = 4.5$ km s^{-1}. The median virial and stellar masses of OB associations are $M_{\rm vir} = 8.9 \times 10^5$ and $M_{\rm st} = 8.1 \times 10^3$ M$_\odot$, respectively. The median star-formation efficiency in parent giant molecular clouds appears to be $\epsilon = 1.2$ per cent. *Gaia* DR2 proper motions confirm the expansion in the Per OB1, Car OB1, and Sgr OB1 associations found earlier with *Gaia* DR1 data. We also detect the expansion in Gem OB1, Ori OB1, and Sco OB1 associations, which became possible for the first time now when analysed with *Gaia* DR2 proper motions. The analysis of the distribution of OB stars in the Per OB1 association shows the presence of a shell-like structure with the radius of 40 pc. Probably, the expansion of the Per OB1 association started with the velocity greater than the present-day expansion velocity equal to 5.0 ± 1.7 km s^{-1}.

Key words: Galaxy: kinematics and dynamics – open clusters and associations – stars: formation.

1 INTRODUCTION

The second intermediate *Gaia* data release (*Gaia* DR2), which is based on the data collected during the first 1.8 yr of *Gaia* mission, provides proper motions for more than 1.3 billion stars with a characteristic accuracy of ∼0.1 mas yr^{-1} (Brown et al. 2018; Katz et al. 2018; Lindegren et al. 2018). The main achievement of *Gaia* DR2 is the large number of stars with high-precision astrometric data.

The first *Gaia* data release (*Gaia* DR1) contains *Tycho-Gaia* Astrometric Solution (TGAS, Michalik, Lindegren & Hobbs 2015; Lindegren et al. 2016) for ∼2 million stars based on positions spanning a 24-yr time interval between *Hipparcos* (ESA 1997) and *Gaia* (Gaia Collaboration 2016) measurements.

Melnik & Dambis (2017) used *Gaia* DR1 (TGAS) data to identify 500 stars in OB associations. These stars have their first-epoch positions determined by the *Hipparcos* catalogue (ESA 1997), which provides the accuracy of TGAS proper motions of ∼0.06 mas yr^{-1}. The average one-dimensional velocity dispersion inside 18 OB associations with more than 10 TGAS stars appeared to be $\sigma_v = 3.9$ km s^{-1}. Precise *Gaia* DR1 (TGAS) proper motions allowed us to find the expansion in the Per OB1, Car OB1, and Sgr OB1 associations determined at significance level $P > 2.5\sigma$ (Melnik & Dambis 2017).

As for the motion of OB associations as whole entities, the results obtained with *Gaia* DR1 and *Gaia* DR2 data are in good agreement. The median velocities of OB associations derived from *Gaia* DR1 and *Gaia* DR2 proper motions differ on average by 2 km s^{-1}. The parameters of the rotation curve calculated with proper motions from *Gaia* DR1 and *Gaia* DR2 are consistent within the errors (Melnik & Dambis 2017; Melnik 2019).

OB associations are sparse groups of O and B stars (Ambartsumian 1949). They are supposed to be born in giant molecular clouds (Elmegreen 1983; Zinnecker & Yorke 2007). There is extensive evidence that giant molecular clouds are in a state close to virial equilibrium (Larson 1981; Krumholz, Matzner & McKee 2006; Kauffmann, Pillai & Goldsmith 2013; Chen et al. 2019). The expected sizes and masses of giant molecular clouds are 10–80 pc and 10^5–2 10^6 M$_\odot$, respectively (Sanders, Scoville & Solomon 1985). The estimate of the average efficiency of star formation, ϵ, in giant molecular clouds defined as the ratio of the total mass of stars born inside a cloud to the initial gas mass lies in the range of 0.1–10 per cent (Myers et al. 1986; Evans et al. 2009; Garcia et al. 2014). The median star-formation efficiency determined for 18 OB associations with more than 10 TGAS stars appears to be 2.1 per cent (Melnik & Dambis 2017).

The radiation of massive stars creates H II regions, which can destroy molecular clouds (McKee 1989; Franco, Shore & Tenorio-Tagle 1994; Colin, Vazquez-Semadeni & Gomez 2013; Kim, Kim & Ostriker 2016). If a gas cloud loses more than 50 per cent of its mass in a time less than one crossing time, then the system becomes unbound (Hills 1980). But if the mass is ejected slowly, then the system can form an expanding OB association with a bound cluster in its centre (Kroupa, Aarseth & Hurley 2001; Boily & Kroupa 2003a, b; Baumgardt & Kroupa 2007).

★ E-mail: anna@sai.msu.ru

The catalogue by Blaha & Humphreys (1989) comprises 91 OB association located within ∼3 kpc of the Sun. Melnik & Efremov (1995) found that many of OB associations identified by Blaha & Humphreys (1989) include several centres of concentration.

The study by Blaauw (1964) stimulated the interest in the search of expanding OB associations. Several methods have been proposed for determining the parameters of expansion in stellar groups (Brown, Dekker & de Zeeuw 1997; Madsen, Dravins & Lindegren 2002). Many studies of expansion of OB associations based on *Gaia* data have been undertaken in the last few years. Kounkel et al. (2018) studied the kinematics of the Ori OB1 association and found significant expansion in only one subgroup inside it. Cantat-Gaudin et al. (2019) studied the Vela OB2 association and detected expansion in all seven detected subgroups. Wright & Mamajek (2018) investigated the Sco OB2 association and found no evidence of expansion inside three selected subgroups. Ward & Kruijssen (2018) identified 18 associations on the basis of their original method and reported that none of them shows evidence of expansion.

Here we do not use *Gaia* DR2 parallaxes for stars of OB associations because they seem to need some correction of their zero-point; moreover, different studies give different values for this correction (Arenou et al. 2018; Lindegren et al. 2018; Riess et al. 2018; Stassun & Torres 2018; Yalyalieva et al. 2018, and other papers). Exception is the Ori OB1 association for which trigonometric and photometric methods give the same distance of 0.4 kpc. Note that associations located at the distances of ∼2 kpc do not show such an agreement. We also do not consider *Gaia* DR2 line-of-sight velocities because they are measured for only 7 per cent of stars of OB associations.

In this paper, we study the internal motions of young stars inside OB associations as derived from *Gaia* DR2 proper motions. Section 2 describes the catalogue of stars in OB associations with *Gaia* DR2 astrometric and photometric data. Section 3 analyses velocity dispersion inside OB associations, determines the virial and stellar masses of OB associations, estimates the star-formation efficiency in giant molecular clouds, and studies the expansion of OB associations and the role of shell-like structures. Section 4 discusses the results and formulates the main conclusions.

2 DATA

The catalogue by Blaha & Humphreys (1989) includes 2209 high-luminosity stars of OB associations, 2007 of them have been identified with *Gaia* DR2 catalogue and 1990 (90 per cent) have *Gaia* DR2 proper motions.

We identified members of OB associations from the catalogue by Blaha & Humphreys (1989) with *Gaia* DR2 stars based on the proximity of stellar coordinates and visual magnitudes. The coordinates in the catalogue by Blaha & Humphreys (1989) are given with small accuracy and therefore we also invoke data from Strasbourg astronomical Data Center.

We cross-matched the list of Blaha & Humphreys (1989) with *Gaia* DR2 catalogue using a matching radius of 3 arcsec and the magnitude tolerance of $|G_{\rm BH} - G| < 3^m$, which gave us matches for a total of 2007 stars. Out of them, the 3-arcsec matches were unique for 1873 stars, 131 stars had two matches, and three stars had three matches. For stars with unique matches, the matching distance did not exceed 0.5 arcsec (the median value is 0.051 arcsec) and for stars with two or three matches, the distance for the closest match did not exceed 0.19 arcsec (the median value is 0.048 arcsec) and the median distances to the second and third matches is 2.01 arcsec, respectively. We therefore adopted all matches where they were unique and adopted the closest match in the remaining cases.

We also compare *Gaia* *G*-band magnitudes with the *G*-band magnitudes ($G_{\rm BH}$) predicted for stars from Blaha & Humphreys (1989) list based on the *B*- and *V*-band data provided in it. The predicted *G*-band values were derived on the basis of an empirical relation involving $(B - V)$ colour indices and *V*-band magnitudes (Jordi et al. 2010):

$$G_{\rm BH} = V - 0.0424 - 0.0851\,(B-V) - 0.3348\,(B-V)^2 + 0.0205\,(B-V)^3. \quad (1)$$

Table 1 (available in the online version of the paper) lists the kinematic and photometric data for stars in OB associations obtained with *Gaia* DR2. It presents the name of a star, the name of the OB association to which it is assigned, spectral type of the star, its luminosity class, and visual magnitude, $m_{\rm v}$, which all are taken from the catalogue by Blaha & Humphreys (1989). We also show the heliocentric distance to the OB association by Blaha & Humphreys (1989), $r_{\rm BH}$, reduced to the short distance scale, $r = 0.8\,r_{\rm BH}$ (Sitnik & Melnik 1996; Dambis, Melnik & Rastorguev 2001; Melnik & Dambis 2009). Table 1 also represents *Gaia* DR2 data: equatorial coordinates, α and δ, of the star, its Galactic coordinates, l and b, the magnitude in the *G*-band, the parallax, π, proper motions along l and b directions, μ_l and μ_b, and their errors, ε_π, ε_{μ_l}, and ε_{μ_b}. It also lists the number of visibility periods, $n_{\rm vis}$, of the star, i. e. the number of groups of observations separated from each other by at least 4 days (Arenou et al. 2018), and the re-normalized unit weight errors (RUWE), which measure how well the *Gaia* observations agree with the five-parameter single-star model and whose large value (RUWE > 1.4) could indicate an astrometric binary (Lindegren 2018, 2019). For completeness, we also added to Table 1 the stellar line-of-sight velocities, V_r, and their errors, $\varepsilon_{\rm vr}$, taken from the catalogue by Barbier-Brossat & Figon (2000), which are available for 52 per cent of stars of OB associations. Here we will consider the refined sample of stars in OB associations including 1771 stars with $n_{\rm vis} > 8$ and RUWE < 1.4. Of 219 excluded stars, 174 stars have RUWE ≥ 1.4 and 45 objects have $n_{\rm vis} \leq 8$.

3 RESULTS

3.1 Velocity dispersion inside OB associations

Let us consider the motions of stars in OB associations in the sky plane. The velocity components of a star along l and b directions, v_l and v_b, are calculated as follows:

$$v_l = 4.74\,\mu_l\,r, \quad (2)$$

$$v_b = 4.74\,\mu_b\,r, \quad (3)$$

where r is the heliocentric distance of the association but μ_l and μ_b are proper motions in mas yr^{-1}. The factor $4.74 \times r$ (kpc) transforms units of mas yr^{-1} into km s^{-1}.

We determine the standard deviations, σ_{vl} and σ_{vb}, of velocity components, v_l and v_b, in an association as half of the velocity interval, Δv_l and Δv_b, including central 68 per cent of member stars with known *Gaia* DR2 proper motions. These robust estimates of the velocity dispersion allow us to minimize the contribution of outliers.

The average uncertainty in determination of proper motions of stars of OB associations in *Gaia* DR2 is 0.086 mas yr^{-1}, which

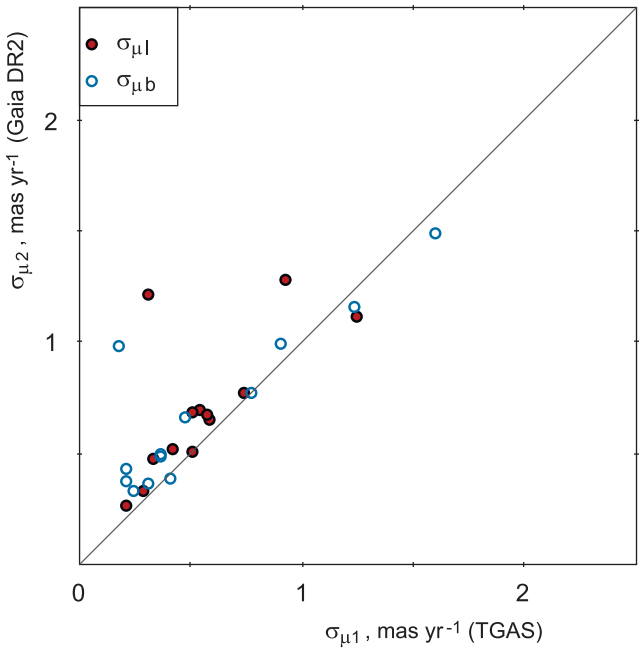

Figure 1. Comparison of the dispersions of the proper motions of stars inside OB associations derived with *Gaia* DR2 and with *Gaia* DR1 (TGAS) data. The solid line shows the bisectrix. We can see that the dispersions obtained with *Gaia* DR2 proper motions are systematically larger than those calculated with *Gaia* DR1. The Cyg OB7 association with the dispersions $\sigma_{\mu 1} = 3.76$ and $\sigma_{\mu 2} = 4.51$ mas yr^{-1} is located beyond the limits of the plot.

corresponds to the uncertainty in the sky-plane velocity of stars at the distance of $r = 1$ kpc equal to 0.4 km s^{-1}.

Fig. 1 compares the dispersions of stellar proper motions inside OB associations derived with *Gaia* DR1 (TGAS) and *Gaia* DR2 data, $\sigma_{\mu 1}$ and $\sigma_{\mu 2}$, respectively. We can see that the dispersions obtained with *Gaia* DR2 proper motions are systematically larger than those calculated with *Gaia* DR1 data. The linear relation between them is $\sigma_{\mu 2} = 1.09 \pm 0.08\,\sigma_{\mu 1}$. Here we consider 13 OB associations with $\sigma_{\mu 2} < 2.5$ mas yr^{-1} and including more than 10 stars common for the *Hipparcos*, *Gaia* DR1, and *Gaia* DR2 catalogues.

Table 2 lists the average standard deviations, $\overline{\sigma_{vl}}$ and $\overline{\sigma_{vb}}$, of velocities, v_l and v_b, inside OB associations, calculated for different samples of member stars with *Gaia* proper motions.

We corrected the velocity dispersions inside OB associations for the inflationary effect of measurement errors by the following way:

$$\sigma_{vl}^2 = \sigma_{l,\,\mathrm{obs}}^2 - (4.74\, r\, \varepsilon_{\mu l})^2, \tag{4}$$

$$\sigma_{vb}^2 = \sigma_{b,\,\mathrm{obs}}^2 - (4.74\, r\, \varepsilon_{\mu b})^2, \tag{5}$$

where $\varepsilon_{\mu l}$ and $\varepsilon_{\mu b}$ are the average errors in determination of proper motions inside an association in the l and b directions, respectively. Table 2 also presents the average velocity dispersions derived for both l and b directions:

$$\overline{\sigma_v} = (\overline{\sigma_{vl}} + \overline{\sigma_{vb}})/2 \tag{6}$$

and the root-mean-square errors in determination of the average velocity dispersions. Table 2 also lists the minimal number of stars, n_μ, with known *Gaia* proper motions, which an association must include for it to be considered in our study, and the number of associations in the sample, n. The comments indicate the criteria for selection of stars in associations. The first four rows are related to *Gaia* DR2 proper motions while the fifth row presents quantities derived from *Gaia* DR1 data. The first and second rows represent samples including associations with more than $n_\mu > 20$ and $n_\mu > 10$ *Gaia* DR2 stars, respectively. The third, fourth, and fifth rows list quantities derived only for stars common for *Hipparcos* and *Gaia* catalogues. The selection of *Hipparcos* stars in *Gaia* DR1 (TGAS) data allows us to use the most precise proper motions (fifth row).

Table 2 suggests that all estimates of the velocity dispersions inside OB associations derived from *Gaia* DR2 data (the first four rows) are greater than those obtained with *Gaia* DR1 (the bottom row). However, the statistical significance of this predominance is not large (just $P \sim 1\,\sigma$). For example, the average velocity dispersion $\overline{\sigma_v}$ calculated for 28 associations with more than $n_\mu > 20$ *Gaia* DR2 proper motions (first row) amounts to 4.46 ± 0.30 km s^{-1} but $\overline{\sigma_v}$ computed for *Gaia* DR1 data is only 3.54 ± 0.49 km s^{-1} (fifth row). Note that the velocity dispersions shown in the fourth and fifth rows are derived on the basis of the same sample of stars and their comparison gives the most convincing argument that the velocity dispersion, $\overline{\sigma_v}$, obtained with *Gaia* DR2 data is greater than $\overline{\sigma_v}$ calculated with *Gaia* DR1 data at a significance level of $P \sim 1\sigma$.

We excluded Cep OB1 ($r = 2.8$ kpc), NGC 2439 ($r = 3.5$ kpc), and R 103 ($r = 3.2$ kpc) associations from consideration because of their distant location from the Sun ($r > 2.8$ kpc), which results in increased probability of wrong membership. Moreover, the Cep OB1 and NGC 2439 associations are very elongated in the l direction and the ratio of their sizes in the l and b directions exceeds $d_l/d_b > 2$, which suggests that they can include a chain of OB associations. The R 103 association has too large velocity dispersion, $\sigma_{vl} = 21$ km s^{-1}, and seems to be strongly contaminated by field stars.

Generally, the observed velocity dispersion inside OB associations has several sources: turbulent motions inside giant molecular clouds, in which young stars were born; motions inside binary systems; and the uncertainty in the determination of proper motions. However, the contribution of the latter source is insignificant.

Here we suppose that the contribution of binary systems into the velocity dispersion inside OB associations is small, no greater than $\sigma_{\mathrm{bn}} \sim 1$ km s^{-1}. Some estimates of the binary effect inside OB associations will be presented in separated paper (Melnik & Dambis, in preparation).

3.2 Efficiency of star formation

Giant molecular clouds, from which OB associations form, seem to be close to their virial equilibrium. The velocity dispersion of turbulent motions, σ_{t}, inside OB association and the radius of association, a, can be used to estimate the virial masses, M_{vir}, of OB associations, which are equal to the masses of their parent molecular clouds:

$$M_{\mathrm{vir}} = \frac{5a\sigma_{\mathrm{t}}^2}{G}, \tag{7}$$

where a is the specific radius of an association. Here we assume a to be the radius containing central 68 per cent of association member stars. The velocity dispersion of turbulent motions, σ_{t}, is supposed to be close to the observed velocity dispersion corrected for measurement errors, σ_v:

$$\sigma_{\mathrm{t}} \approx \sigma_v. \tag{8}$$

Another remark is connected with the expansion of the Car OB1 and Per OB1 associations, which had a considerably smaller size some time ago – this seems to be their initial size – so their present-

Table 2. Average velocity dispersion inside OB associations.

Row	Catalogue	Condition	$\overline{\sigma_{vl}}$ (km s^{-1})	$\overline{\sigma_{vb}}$ (km s^{-1})	$\overline{\sigma_{v}}$ (km s^{-1})	n	Comments
1	*Gaia* DR2	$n_\mu > 20$	4.96 ± 0.49	3.96 ± 0.36	4.46 ± 0.30	28	Stars identified with *Gaia* DR2
2	*Gaia* DR2	$n_\mu > 10$	4.65 ± 0.39	4.69 ± 0.33	4.17 ± 0.26	40	Stars identified with *Gaia* DR2
3	*Gaia* DR2	$n_\mu > 10$	4.69 ± 0.49	3.96 ± 0.47	4.33 ± 0.34	23	Common stars for *Gaia* DR2 and *Hipparcos*
4	*Gaia* DR2	$n_\mu > 10$	5.30 ± 0.88	4.42 ± 0.81	4.86 ± 0.60	14	Common stars for *Gaia* DR1, DR2 and *Hipparcos*
5	*Gaia* DR1	$n_\mu > 10$	3.77 ± 0.64	3.30 ± 0.75	3.54 ± 0.49	16	Common stars for *Gaia* DR1 and *Hipparcos*

Table 3. Virial and stellar masses of OB associations, $M_{\rm vir}$ and M_{st}, and star formation efficiency ϵ.

Name	l (deg)	b (deg)	r (kpc)	V_r (km s^{-1})	σ_{vl} (km s^{-1})	σ_{vb} (km s^{-1})	a (kpc)	n_μ	$M_{\rm vir}$ M$_\odot$	$M_{\rm st}$ M$_\odot$	N_{20}	ϵ 100 per cent
SGR OB5	0.04	− 1.16	2.42	− 15.0 (2)	13.4	7.0	0.068	27	83.2×10^5	7.5×10^3	18	0.1
SGR OB1	7.54	− 0.77	1.26	− 10.0 (37)	2.5	5.0	0.037	47	6.0×10^5	9.2×10^3	22	1.5
SER OB1	16.71	0.07	1.53	-5.0 (17)	4.0	4.0	0.051	33	9.7×10^5	8.3×10^3	20	0.9
CYG OB3	72.76	2.04	1.83	− 10.0 (29)	6.8	4.1	0.024	32	8.5×10^5	10.8×10^3	26	1.3
CYG OB1	75.84	1.12	1.46	− 13.5 (34)	6.2	3.6	0.032	62	9.0×10^5	16.7×10^3	40	1.8
CYG OB9	77.81	1.80	0.96	− 19.5 (10)	3.4	3.4	0.017	22	2.3×10^5	4.6×10^3	11	2.0
CYG OB8	77.92	3.36	1.83	− 21.0 (9)	4.7	9.5	0.040	20	23.5×10^5	6.7×10^3	16	0.3
CYG OB7	88.98	0.03	0.63	-9.4 (21)	11.0	2.2	0.051	22	25.7×10^5	2.9×10^3	7	0.1
CEP OB2	102.02	4.69	0.73	− 17.0 (36)	5.3	4.7	0.046	45	13.5×10^5	7.9×10^3	19	0.6
CAS OB2	111.99	− 0.00	2.10	− 50.1 (7)	7.8	6.5	0.056	30	33.4×10^5	9.6×10^3	23	0.3
CAS OB5	116.09	− 0.50	2.01	− 45.8 (16)	3.6	3.7	0.043	45	6.7×10^5	9.6×10^3	23	1.4
CAS OB4	120.05	− 0.30	2.30	− 37.0 (7)	7.8	5.3	0.070	24	34.9×10^5	5.4×10^3	13	0.2
CAS OB7	122.98	1.22	2.01	− 50.0 (4)	3.7	2.4	0.041	35	4.6×10^5	6.7×10^3	16	1.5
CAS OB8	129.16	− 1.06	2.30	− 34.6 (14)	1.7	2.1	0.037	41	1.6×10^5	8.3×10^3	20	5.3
PER OB1	134.70	− 3.14	1.83	− 43.2 (80)	3.7	2.9	0.064	150	5.7×10^5	36.2×10^3	87	6.4[a]
CAS OB6	134.95	0.72	1.75	− 42.6 (12)	4.6	5.9	0.057	29	18.5×10^5	6.7×10^3	16	0.4
CAM OB1	141.08	0.89	0.80	− 11.0 (30)	3.3	2.9	0.079	41	8.8×10^5	5.0×10^3	12	0.6
AUR OB1	173.83	0.14	1.06	-1.9 (26)	4.0	3.0	0.072	31	10.2×10^5	3.7×10^3	9	0.4
ORI OB1	206.90	− 17.71	0.40	25.4 (62)	2.9	1.7	0.035	54	2.2×10^5	3.3×10^3	8	1.5
GEM OB1	188.96	2.22	1.21	16.0 (18)	3.8	2.5	0.042	35	4.8×10^5	5.4×10^3	13	1.1
MON OB2	207.35	− 1.60	1.21	23.0 (25)	3.3	4.0	0.037	23	5.6×10^5	5.4×10^3	13	1.0
VELA OB1	264.83	− 1.41	1.46	23.0 (18)	4.1	3.5	0.057	43	9.5×10^5	10.4×10^3	25	1.1
CAR OB1	286.45	− 0.46	2.01	-5.0 (39)	7.6	3.2	0.064	101	15.5×10^5	20.8×10^3	50	1.3[a]
CAR OB2	290.39	0.12	1.83	-8.2 (22)	3.8	2.6	0.028	48	3.3×10^5	10.4×10^3	25	3.1
CRU OB1	294.87	− 1.06	2.01	-5.3 (33)	4.1	2.5	0.040	65	5.1×10^5	9.6×10^3	23	1.9
CEN OB1	304.14	1.44	1.92	− 19.0 (32)	5.1	2.9	0.068	85	12.5×10^5	20.4×10^3	49	1.6
ARA OB1A	337.68	− 0.92	1.10	− 36.3 (8)	4.6	7.8	0.046	42	20.6×10^5	4.6×10^3	11	0.2
SCO OB1	343.72	1.37	1.53	− 28.8 (28)	2.1	2.3	0.013	66	0.8×10^5	11.7×10^3	28	15.0

[a] Values of $M_{\rm vir}$ and ϵ for the Per OB1 and Car OB1 associations are corrected for the expansion effect (Section 3.3).

day radius a must be corrected by a factor:

$$a_{\rm c} = a\,\xi, \tag{9}$$

where ξ is the ratio of the minimum to the present-day radius of an association (see Section 3.4, equation 29).

We can also calculate the stellar masses of OB associations, $M_{\rm st}$, through the number of stars with masses greater than 20 M$_\odot$, N_{20}. Note that Blaha & Humphreys (1989) considered the catalogue of stars in OB associations to be fairly complete for stars brighter than $M_{\rm bol} < -7.5^m$, which corresponds to stars with masses greater than ∼20 M$_\odot$ (Bressan et al. 2012). The power law mass function by Kroupa (2002) calibrated via N_{20} can be used to estimate the full mass of stars in an association (for more details, see Melnik & Dambis 2017).

Table 3 lists the virial and stellar masses, $M_{\rm vir}$ and $M_{\rm st}$, of OB associations containing more than 20 stars with *Gaia* DR2 proper motions, $n_\mu > 20$. It also lists the general parameters of an OB association: the average Galactic longitude and latitude, l and b; the average heliocentric distance, r; the median line-of-sight velocity, V_r, and the number of stars it is derived from given in parentheses; the specific radius of OB association, a; the number of stars with masses $M > 20$ M$_\odot$, N_{20}; the velocity dispersions in l and b directions, σ_{vl} and σ_{vb}; and the number of stars with known *Gaia* DR2 proper motions, n_μ. Also listed in Table 3 is the average efficiency of star formation, ϵ, inside the parent giant molecular cloud:

$$\epsilon = M_{\rm st}/M_{\rm vir}. \tag{10}$$

Table 3 indicates that the star formation efficiency in OB associations ranges from 0.1 to 15 per cent. Its median value calculated for 28 OB associations is $\epsilon = 1.2$ per cent. The median virial and stellar masses appear to be 8.9×10^5 and 8.1×10^3 M$_\odot$, respectively.

3.3 Expansion of OB associations

We determine possible expansion or compression of OB associations via parameters p_l and p_b:

Table 4. Expansion/compression of OB associations with *Gaia* DR2 proper motions.

Name	p_l (km s^{-1} kpc^{-1})	p_b (km s^{-1} kpc^{-1})	a (kpc)	u_l (km s^{-1})	u_b (km s^{-1})	e_1 (km s^{-1})	$\tilde{u}_l$ (km s^{-1})	$\tilde{u}_b$ (km s^{-1})	n_μ
SGR OB5	64 ± 63	−4 ± 25	0.068	4.4 ± 4.3	−0.3 ± 1.7	0.43 ± 0.10	4.0 ± 4.3	−0.7 ± 1.7	27
SGR OB1	−13 ± 11	145 ± 36	0.037	−0.5 ± 0.4	5.3 ± 1.3	0.29 ± 0.05	−0.8 ± 0.4	5.0 ± 1.3	47
SER OB1	−1 ± 33	44 ± 41	0.051	−0.1 ± 1.7	2.2 ± 2.1	0.17 ± 0.12	−0.2 ± 1.7	2.1 ± 2.1	33
CYG OB3	249 ± 109	139 ± 67	0.024	6.1 ± 2.6	3.4 ± 1.6	0.13 ± 0.02	5.9 ± 2.6	3.3 ± 1.6	31
CYG OB1	−5 ± 68	25 ± 35	0.032	−0.2 ± 2.2	0.8 ± 1.1	0.30 ± 0.02	−0.5 ± 2.2	0.5 ± 1.1	62
CYG OB9	162 ± 85	113 ± 176	0.017	2.8 ± 1.5	2.0 ± 3.0	0.35 ± 0.03	2.5 ± 1.5	1.6 ± 3.0	22
CYG OB8	−46 ± 93	178 ± 47	0.040	−1.8 ± 3.7	7.1 ± 1.9	0.46 ± 0.05	−2.3 ± 3.7	6.7 ± 1.9	19
CYG OB7	−67 ± 69	122 ± 51	0.051	−3.4 ± 3.5	6.2 ± 2.6	0.76 ± 0.16	−4.1 ± 3.5	5.4 ± 2.6	22
CEP OB2	72 ± 27	14 ± 22	0.046	3.4 ± 1.2	0.6 ± 1.0	1.09 ± 0.06	2.3 ± 1.2	−0.4 ± 1.0	45
CAS OB2	−32 ± 58	121 ± 33	0.056	−1.8 ± 3.2	6.8 ± 1.8	1.34 ± 0.05	−3.1 ± 3.2	5.4 ± 1.8	29
CAS OB5	54 ± 32	49 ± 22	0.043	2.3 ± 1.4	2.1 ± 1.0	0.99 ± 0.02	1.3 ± 1.4	1.1 ± 1.0	45
CAS OB4	95 ± 55	63 ± 20	0.070	6.7 ± 3.8	4.4 ± 1.4	1.13 ± 0.05	5.6 ± 3.8	3.3 ± 1.4	22
CAS OB7	74 ± 27	63 ± 35	0.041	3.0 ± 1.1	2.6 ± 1.4	1.02 ± 0.00	2.0 ± 1.1	1.6 ± 1.4	34
CAS OB8	51 ± 17	37 ± 19	0.037	1.9 ± 0.6	1.4 ± 0.7	0.56 ± 0.02	1.3 ± 0.6	0.8 ± 0.7	40
PER OB1	51 ± 9	65 ± 10	0.064	3.3 ± 0.6	4.2 ± 0.6	1.52 ± 0.02	1.8 ± 0.6	2.7 ± 0.6	149
CAS OB6	89 ± 30	185 ± 39	0.057	5.1 ± 1.7	10.6 ± 2.2	1.39 ± 0.05	3.7 ± 1.7	9.2 ± 2.2	28
CAM OB1	36 ± 14	−21 ± 17	0.079	2.8 ± 1.1	−1.6 ± 1.3	1.08 ± 0.14	1.7 ± 1.1	−2.7 ± 1.3	41
AUR OB1	11 ± 14	−8 ± 15	0.072	0.8 ± 1.0	−0.6 ± 1.1	0.13 ± 0.17	0.7 ± 1.0	−0.7 ± 1.1	31
ORI OB1	−15 ± 14	−57 ± 16	0.035	−0.5 ± 0.5	−2.0 ± 0.5	−2.21 ± 0.09	1.7 ± 0.5	0.2 ± 0.5	54
GEM OB1	10 ± 34	77 ± 26	0.042	0.4 ± 1.4	3.2 ± 1.1	−0.55 ± 0.03	1.0 ± 1.4	3.8 ± 1.1	35
MON OB2	−215 ± 45	36 ± 66	0.037	−7.9 ± 1.6	1.3 ± 2.4	−0.70 ± 0.07	−7.2 ± 1.6	2.0 ± 2.4	23
VELA OB1	26 ± 22	−29 ± 16	0.057	1.5 ± 1.2	−1.7 ± 0.9	−0.89 ± 0.03	2.4 ± 1.2	−0.8 ± 0.9	42
CAR OB1	101 ± 14	37 ± 14	0.064	6.5 ± 0.9	2.4 ± 0.9	0.16 ± 0.03	6.3 ± 0.9	2.2 ± 0.9	100
CAR OB2	59 ± 59	83 ± 27	0.028	1.6 ± 1.6	2.3 ± 0.8	0.13 ± 0.02	1.5 ± 1.6	2.2 ± 0.8	48
CRU OB1	35 ± 31	33 ± 16	0.040	1.4 ± 1.2	1.3 ± 0.6	0.11 ± 0.02	1.3 ± 1.2	1.2 ± 0.6	64
CEN OB1	−18 ± 18	13 ± 11	0.068	−1.2 ± 1.2	0.9 ± 0.7	0.67 ± 0.06	−1.9 ± 1.2	0.2 ± 0.7	84
ARA OB1A	31 ± 31	82 ± 39	0.046	1.4 ± 1.4	3.7 ± 1.8	1.51 ± 0.13	−0.1 ± 1.4	2.2 ± 1.8	42
SCO OB1	224 ± 29	142 ± 38	0.013	3.0 ± 0.4	1.9 ± 0.5	0.25 ± 0.02	2.8 ± 0.4	1.7 ± 0.5	66

$$v_l = v_{l0} + p_l\, r \sin(l - l_0), \tag{11}$$

$$v_b = v_{b0} + p_b\, r \sin(b - b_0), \tag{12}$$

where $v_{l\,0}$ and $v_{b\,0}$ are the average velocities of the association; l_0 and b_0 are the coordinates of the centre of the group; and parameters p_l and p_b characterize expansion (positive values) or compression (negative values) along the l or b direction, respectively. We solve the systems of equations (11) and (12) for all member stars of an association with known *Gaia* DR2 proper motions to determine the values of p_l and p_b.

The observed specific velocities of expansion or compression, u_l and u_b, are computed as:

$$u_l = p_l\, a, \qquad u_b = p_b\, a. \tag{13}$$

The motion of an OB association as a whole with line-of-sight velocity V_r can also produce the effect of spurious expansion/compression, which creates the expansion/compression with the specific velocity e_1:

$$e_1 = -V_r\, \frac{a}{r}, \tag{14}$$

where a and r are the specific radius and heliocentric distance of the OB association, respectively (for example, Melnik & Dambis 2018). The motion of a group toward the Sun ($V_r < 0$) produces spurious expansion ($e_1 > 0$) while the motion away from the Sun ($V_r > 0$) creates spurious compression ($e_1 < 0$). Generally, the observed velocities, u_l and u_b, must be corrected for this effect:

$$\tilde{u}_l = u_l - e_1, \qquad \tilde{u}_b = u_b - e_1. \tag{15}$$

Here we use the median values of line-of-sight velocities of OB associations, V_r (Table 3), which are derived from the velocities of individual stars taken from the catalogue by Barbier-Brossat & Figon (2000).

Table 4 lists the parameters of expansion/compression, p_l and p_b, the velocities u_l, u_b, e_1, $\tilde{u}_l$, $\tilde{u}_b$, and their uncertainties for 28 OB associations containing more than 20 stars with *Gaia* DR2 proper motions. We will discuss only velocities $\tilde{u}_l$ or $\tilde{u}_b$ determined at a significance level greater than $P > 3\sigma$, which are underlined in Table 4.

Fig. 2 shows distribution of observed relative velocities, V_l' and V_b', determined with respect to the centre of the group:

$$V_l' = v_l - v_{l0}, \tag{16}$$

$$V_b' = v_b - v_{b0}, \tag{17}$$

in five OB associations: Sgr OB1, Per OB1, Gem OB1, Car OB1, and Sco OB1, which demonstrate significant expansion in both cases: in the observed relative velocities and after their correction for the motion of the group as a whole. Four other associations (Ori OB1, Cyg OB8, Cas OB2, and Mon OB2) will be discussed below.

Here we excluded from consideration 17 member stars with the absolute values of the relative velocities, V_l' or V_b', greater than 50 km s^{-1}, because such large velocities cannot be connected with expansion of OB associations and are possibly due to binary systems or runaway stars (Fujii & Portegies Zwart 2011, see Appendix A).

Fig. 2 also indicates the positions of O-type stars, which are the youngest in OB associations. We can see that O-type stars are distributed more or less uniformly among other stars of OB associations.

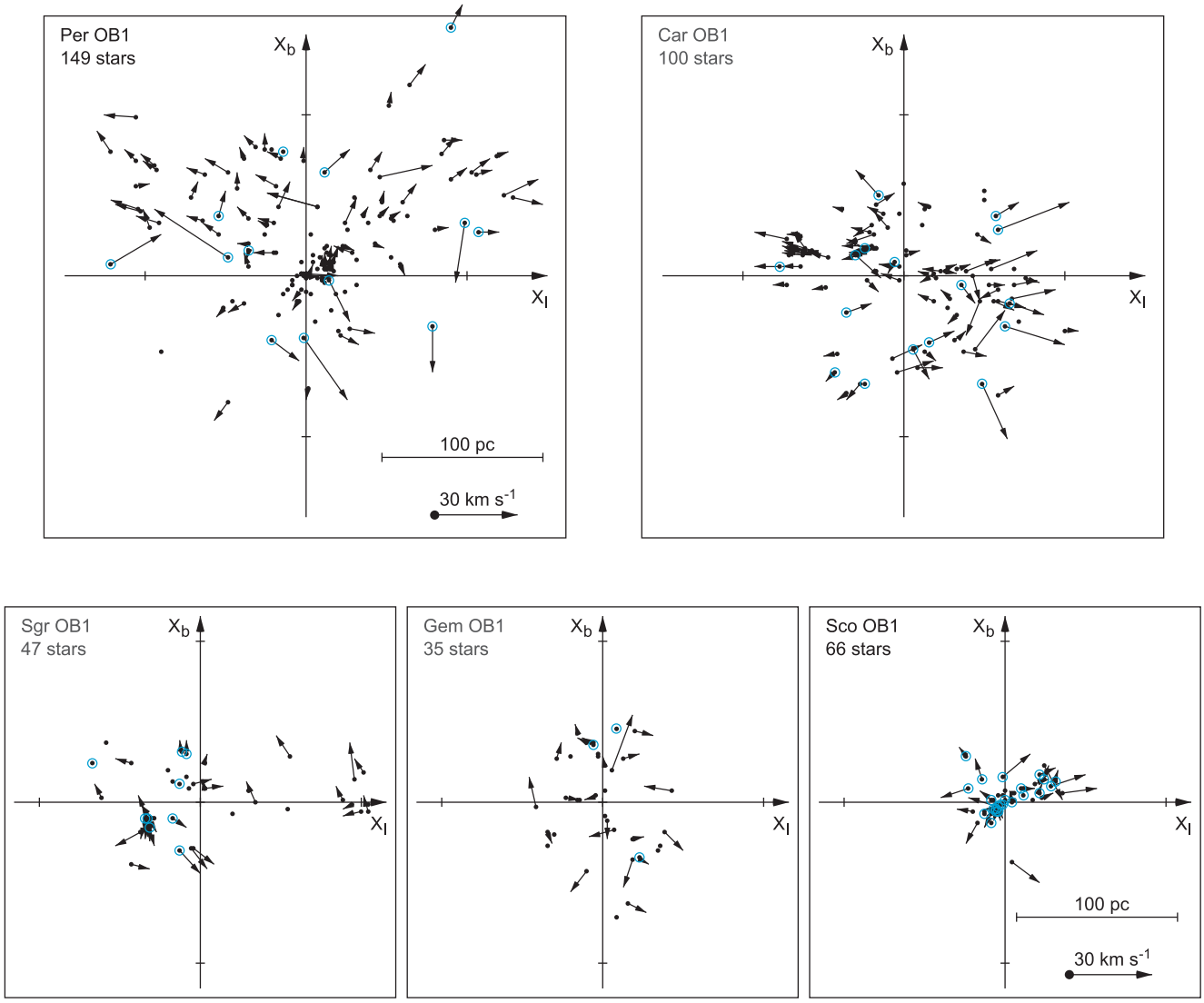

Figure 2. Distribution of observed relative velocities, V_l' and V_b', in the Per OB1, Car OB1, Sgr OB1, Gem OB1, and Sco OB1 associations. All frames have the same scale. The velocities V_l' and V_b' are determined with respect to the centre of the association (equations 16 and 17). Stars with the relative velocities $|V_l'|$ and $|V_b'|$ smaller than 3 km s^{-1} are shown as black circles without any vector. The axes X_l and X_b are directed towards increasing values of Galactic coordinates, l and b, respectively. We can see conspicuous expansion in these associations. Stars of spectral type O are outlined by circles (coloured blue in online article). O-type stars can be seen to be distributed more or less uniformly among other stars of OB associations.

Fig. 2 shows that the Sgr OB1 association includes several groups of stars moving in opposite directions along the X_b-axis. We do not observe here the expansion from one point as it is, for example, in the Per OB1 or Car OB1 association. The method of cluster analysis also shows that Sgr OB1 includes at least two different groups (Melnik & Efremov 1995).

As for Gem OB1, it is just the exclusion of five stars with the error RUWE $>$ 1.4 from consideration that allows us to find the expansion inside this association.

Fig. 3 shows the distribution of relative velocities in the Ori OB1 association: Fig. 3(a) displays the observed relative velocities, whereas Fig. 3(b) shows the velocities corrected for the motion of the association as a whole, V_{lc}' and V_{bc}':

$$V_{lc}' = V_l' + V_r \frac{X_l}{r}, \tag{18}$$

$$V_{bc}' = V_b' + V_r \frac{X_b}{r}, \tag{19}$$

where the pair (X_l, X_b) are the coordinates of a star in the sky plane measured from the centre of OB association along l and b directions, respectively. The velocity corrections are zero at the centre of the group and increase towards its periphery. The velocity of spurious expansion, e_1 (equation 14), in the Ori OB1 association is quite large in absolute value, $e_1 = -2.2$ km s^{-1} (Table 4), which is due to its location near the Sun ($r = 0.4$ kpc) and its large line-of-sight velocity, $V_r = +25.4$ km s^{-1}, resulting from a combined contribution due to the solar motion to the apex ($+13$ km s^{-1}), the rotation curve ($+5$ km s^{-1}), and the residual velocity ($+7$ km s^{-1}). Note that the motion of the Ori OB1 association away from the Sun produces spurious compression. Fig. 3 shows that after the correction for the spurious compression, the relative velocities demonstrate small expansion in the l direction.

To check the expansion of the Ori OB1 association, we analyse the distribution of relative velocities in the (X_l, X_r) plane, where the X_r-axis is directed along the line of sight connecting the Sun

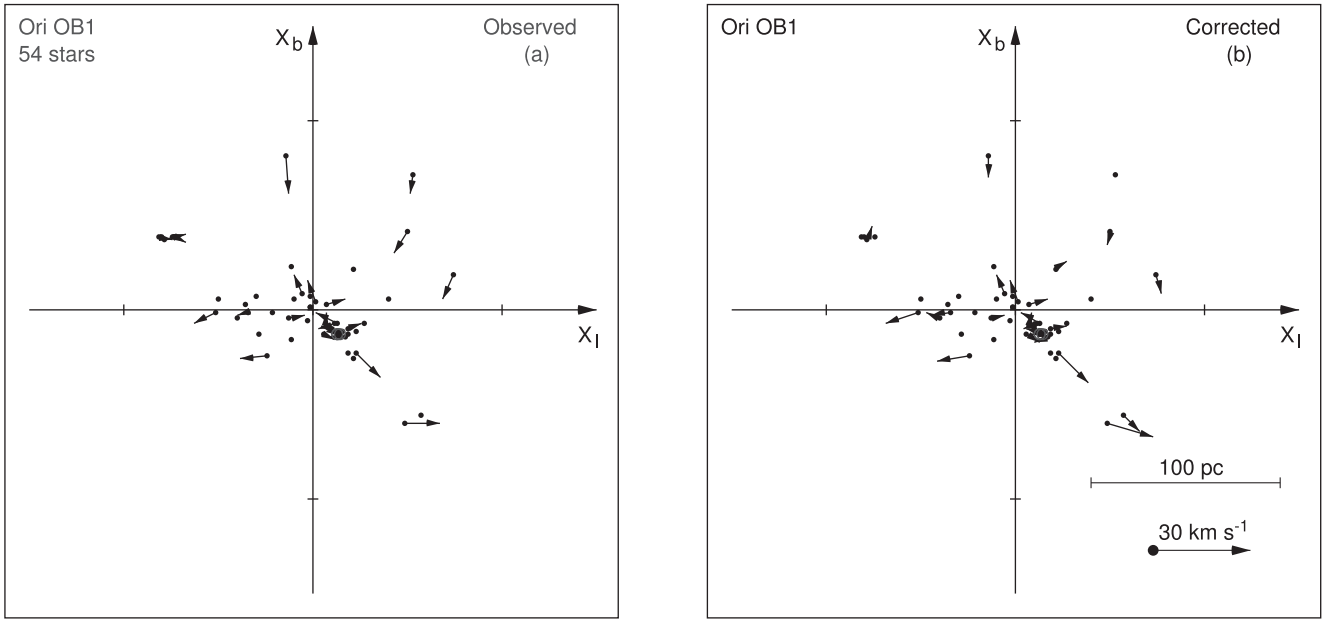

Figure 3. Distribution of (a) observed, V_l' and V_b', and (b) corrected, V_{lc}' and V_{bc}' (equations 18 and 19), relative velocities in the Ori OB1 association. Stars with the relative velocities $|V_l'|$ and $|V_b'|$ smaller than 3 km s^{-1} are shown as black circles without any vector. The axes X_l and X_b point in the l and b directions, respectively. We can see small expansion along the X_l-axis in the distribution of relative velocities corrected for the motion of the association as a whole.

and the centre of the Ori OB1 association (Fig. 4). The coordinate X_r and the relative velocity V_r' of a star are derived from the *Gaia* DR2 parallax, π, and the stellar line-of-sight velocity, V_r, in the following way:

$$X_r = \frac{1}{\pi}\cos\phi - \frac{1}{\pi_0}, \tag{20}$$

$$V_r' = V_r\cos\phi - V_{r0}, \tag{21}$$

where π_0 is the median parallax of stars of the Ori OB1 association; $V_{r\,0}$ is the average stellar line-of-sight velocity projected on to the X_r direction, and the angle ϕ is the heliocentric angle between the direction to the star and to the centre of the association:

$$\phi = \arctan\frac{\sqrt{X_l^2 + X_b^2}}{r}, \tag{22}$$

which takes values in the range $|\phi| < 13^\circ$.

The parameter of expansion in the X_r direction, p_r, is determined by solving the equation:

$$V_r' = p_r\, X_r. \tag{23}$$

Fig. 4 shows conspicuous expansion of the Ori OB1 association along the line of sight. The parameter of expansion appears to be $p_r = 105 \pm 29$ km s^{-1} kpc $^{-1}$, which corresponds to the specific velocity of expansion, u_r:

$$u_r = p_r\, a, \tag{24}$$

equal to $u_r = 3.6 \pm 1.0$ km s^{-1}. Here we use the line-of-sight velocities, V_r, and parallaxes, π, measured with the uncertainties less than 5 km s^{-1} and 0.2 mas, respectively, which are available for 36 stars of the Ori OB1 association. The stellar line-of-sight velocities are taken from the catalogue by Barbier-Brossat & Figon (2000).

We found that the expansion/compression in the Cyg OB8, Cas OB2, and Mon OB2 associations relies on the velocities of only a few stars. The exclusion of ∼10 per cent of stars with *Gaia* DR2 proper motions from these associations (HD 191423 and HD 191778 from Cyg OB8; BD + 63 1964 from Cas OB2; and HD 262042, HD 47732, and HD 47777 from Mon OB2) decreases the absolute value of expanding/compressing velocity, $\tilde{u}_l$ or $\tilde{u}_b$, down to a significance level of less than 2σ.

Fig. 5 shows the dependence of the stellar proper motions, μ_l and μ_b, on the coordinates l and b, respectively, for the associations Sgr OB1, Gem OB1, Ori OB1, Per OB1, Car OB1, and Sco OB1. Also shown is the expected dependence due to the motion of the association as a whole. We can see that in all cases except Ori OB1, the correlation between μ_l and l or between μ_b and b is positive and greater than the correlation due to spurious expansion. Positive correlation between the coordinate and corresponding proper motion suggests expansion, whereas negative correlation means compression. The Ori OB1 association is a special case – here one expects to see considerable negative correlation between μ_l and l (the dashed line) caused by the motion of the association away from the Sun with $V_r = 25$ km s^{-1}, but the observed dependence (the red line) is much weaker than the expected one, which indicates the presence of some physical expansion practically compensating its spurious compression.

3.4 Kinematic ages of OB associations

We can make crude estimates of stellar ages on the basis of their spectral types (effective temperatures) and luminosities using available stellar models and various photometric calibrations. The ages of O8 stars of all luminosity classes must be smaller than 5 Myr, while B0 stars must be younger than 10 Myr (Bressan et al. 2012). So the ages of OB associations are supposed to be 5–10 Myr. However, the low-mass stars born in the same molecular cloud can be conspicuously older and some estimates of their ages are as old as 20–50 Myr (Pecaut & Mamajek 2016; Cantat-Gaudin et al. 2019). In this context, it is interesting to compare the ages of OB associations

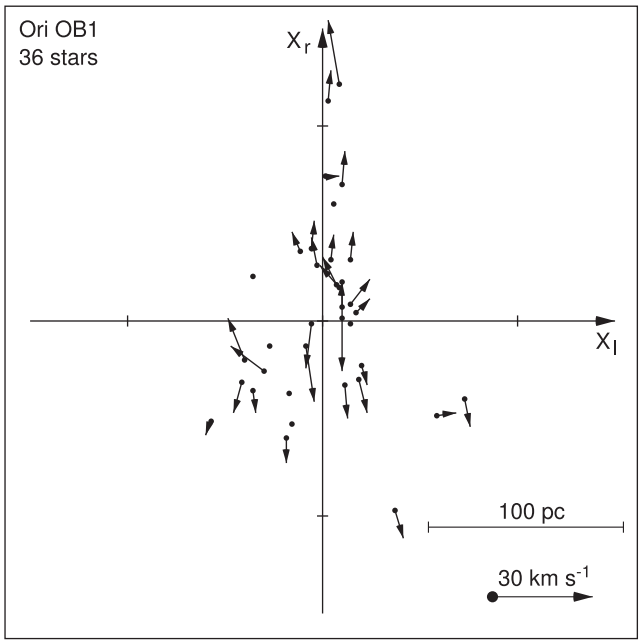

Figure 4. Distribution of relative velocities, V'_{lc} and V'_r, in the plane (X_l, X_r), where the axes X_l and X_r point in the l direction and along the line of sight connecting the Sun and the centre of the Ori OB1 association, respectively. The Sun is at the bottom. The velocity V'_r is the relative velocity along the line of sight (equation 21). The velocity V'_{lc} is the relative velocity in the l direction corrected for the motion of the association as a whole (equation 18). Stars with the relative velocities $|V'_{lc}|$ and $|V'_r|$ smaller than 3 km s^{-1} are shown as black circles without any vector. We can see conspicuous expansion of the Ori OB1 association along the line of sight here.

derived from stellar models (the so-called stellar ages) with their kinematic ages, i.e. the time instants in the past when the group had minimal size. There are two classical methods of the determination of kinematic ages. One method derives the kinematic ages from p_l and p_b, while another is based of the backtracking the positions of individual stars. Brown et al. (1997) tested both methods and found that the first method overestimates the kinematic age while the second method, on the contrary, underestimates it.

Table 5 presents the estimates of the kinematic ages determined by two different ways. The values T_l and T_b are computed by the first method through the values of p_l, p_b, e_1 and a:

$$T_l = \left[\left(p_l - \frac{e_1}{a}\right) f_v\right]^{-1}, \tag{25}$$

$$T_b = [(p_b - \frac{e_1}{a})\, f_v]^{-1}, \tag{26}$$

where factor $f_v = 1.023 \times 10^{-3}$ transforms velocities in units of km s^{-1} into kpc Myr^{-1}. The parameters of expansion, p_l and p_b, were corrected for the motion of the association as a whole.

The second method is based on the positions and proper motions of individual stars. We determine the positions of member stars in the past using their present-day coordinates and velocities. Here we suppose that stars in an association start their expansion at one moment in the past but with different velocities. The observed velocities computed with respect to the centre of the association, v'_l and v'_b, were corrected for the motion of the association as a whole:

$$x(t) = x_0 - \left(v'_l + V_r \frac{x_0}{r}\right) t, \tag{27}$$

$$y(t) = y_0 - \left(v'_b + V_r \frac{y_0}{r}\right) t. \tag{28}$$

The selection of the most compact part of association allows us to mitigate changes due to inclusion or exclusion of individual stars. Only cases with well-defined expansion are considered.

Fig. 6 shows the dependence of the size of OB association, s, on the time t in the past. The value s is the radius of the association containing central 68 per cent of its members with known *Gaia* proper motions. Note that the second method is very sensitive to the errors in proper motions of individual stars. So we select stars with the most precise proper motions in the Per OB1 association and calculate function $s(t)$ for this sample as well. The new sample includes stars with $\varepsilon_{\mu l} < 0.008$ mas yr^{-1} and $\varepsilon_{\mu b} < 0.008$ mas yr^{-1} leaving 38 stars in the Per OB1 association.

Fig. 6 shows that function $s(t)$ has a minimum in some cases and a plateau with subsequent growth in others. In the Per OB1 association, the sample of stars with the most precise proper motions shows minimum on the curve $s(t)$ while the sample including all stars with *Gaia* DR2 proper motions gives a plateau. The selection of stars with the most accurate proper motions does not change the results in the Sgr OB1, Car OB1, and Sco OB1 associations, so we do not demonstrate them separately. Note that the average uncertainty in determination of *Gaia* DR2 proper motions in the Ori OB1 association is $\varepsilon_{\mu l} = 0.230$ mas yr^{-1}, and the criteria considered leave no stars here.

Kinematic ages of OB associations obtained by the second method, T^*, correspond to the minimum on the curves $s(t)$. Note that a considerable difference between the minimum and present-day sizes of an association:

$$\xi = s(T_l^*)/s(0) \tag{29}$$

is observed only in the Per OB1 and Car OB1 associations equal to $\xi = 0.69$ and $\xi = 0.73$, respectively. The minimal radii of OB associations corresponding to the plateau or to a minimum of functions $s(t)$ are: 67 pc (Per OB1), 47 pc (Car OB1), 10 pc (Sco OB1), 35 pc (Sgr OB1), and 29 pc (Ori OB1). These values are located in the interval 10–100 pc corresponding to the expected sizes of giant molecular clouds (Sanders et al. 1985).

Table 5 lists the kinematic ages T^* and their errors calculated from the uncertainties in proper motions that cause the uncertainties in the determination of sizes of OB associations, Δs, proportional to the time interval in the past:

$$\Delta s = 4.74\, r\, \varepsilon_\mu\, T^*\, f_v, \tag{30}$$

where ε_μ is the average uncertainty in determination of proper motions in l and b directions. The values of Δs are as follows: 4 pc (Per OB1, sample of stars with the most precise proper motions), 2 pc (Car OB1, Sco OB1, Gem OB1), and 1 pc (Sgr OB1, Ori OB1).

In the case of Sgr OB1, we can give only upper limit for the value of T^*. The values of T^* do not exceed 4 Myr except the case of the Per OB1 association where it amounts to $T^* = 10.6^{+2.6}_{-3.9}$ Myr.

Table 5 suggests that the kinematic ages, T_l and T_b, obtained by the first method are always greater than corresponding estimates derived using the second method, T^*, which agrees with the results by Brown et al. (1997). The first method (equations 25 and 26) is less sensitive to the errors in proper motions of individual stars: several erroneous proper motions cannot spoil the picture of overall expansion (Fig. 5), but this method assumes that the OB association expands from a point or from a very small region, which can be incorrect in some cases. The second method (equations 27 and 28) is more direct: it does not involve additional assumptions about the initial size of the group, but it is more sensitive to the errors in proper motions of individual stars, which can completely wash out the expansion (Fig. 6).

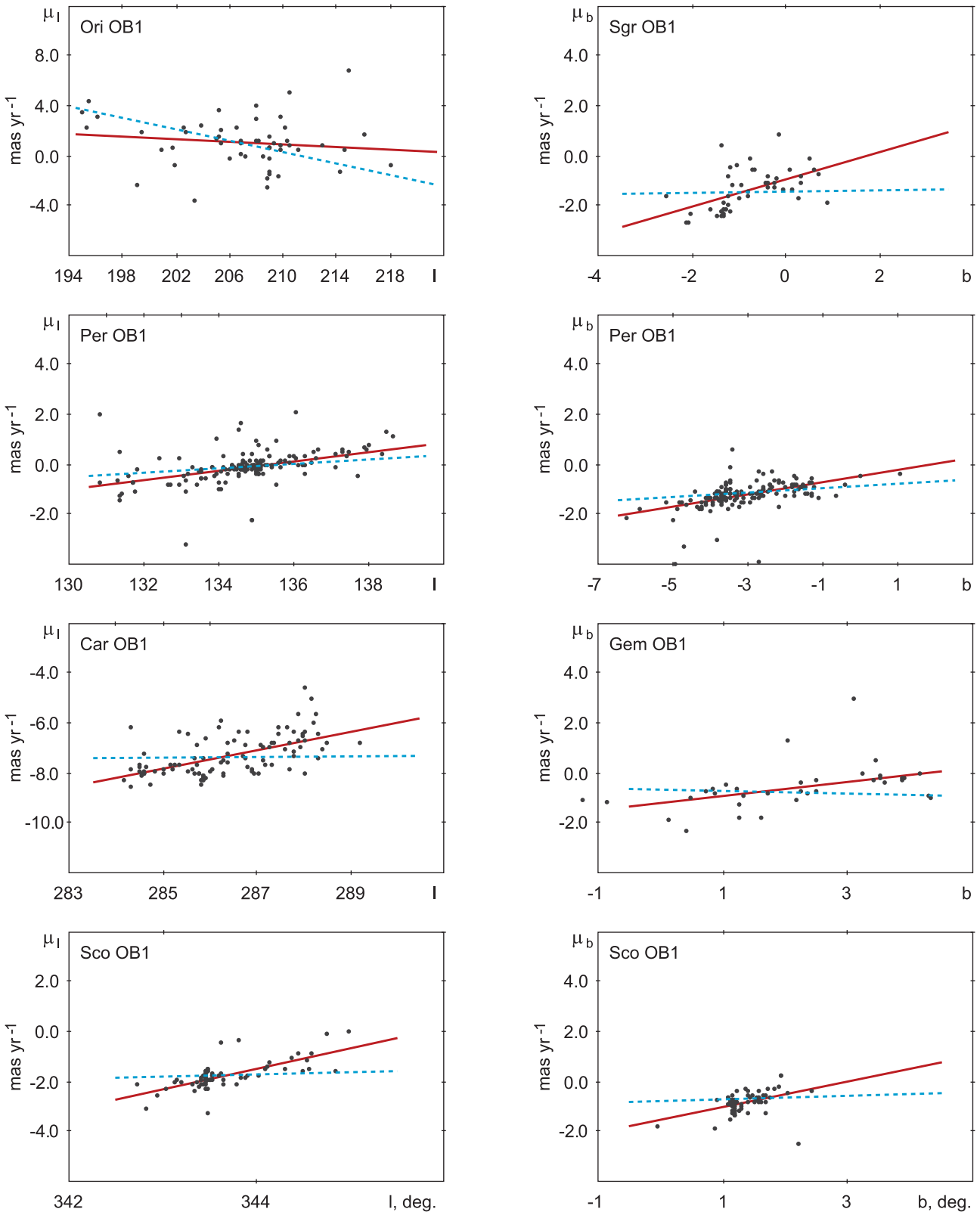

Figure 5. Dependence of stellar proper motion components, μ_l and μ_b, on the corresponding coordinates, l and b, in the associations Sgr OB1, Per OB1, Ori OB1, Gem OB1, Car OB1, and Sco OB1. The solid lines (coloured red in the online article) indicate the linear fits of the dependencies μ_l (l) and μ_b (b) determined from observational data while the dashed lines (coloured blue in the online article) show the correlation between μ_l and l or between μ_b and b, which appears due to the motion of the association as a whole (equation 14). Positive correlation between the proper motion and corresponding coordinate means expansion while negative correlation indicates compression. In the Ori OB1 association, the spurious compression due to its motion along the line of sight is considerably larger than that derived from the observed data, which suggests the presence of a physical expansion.

Table 5. Kinematic ages of OB associations.

Name	T_l Myr	T_b Myr	T^* Myr
Sgr OB1	–	$7.1^{+0.6}_{-1.5}$	<1
Per OB1	36^{+17}_{-8}	24^{+7}_{-5}	$10.6^{+2.6}_{-3.9}$
Ori OB1	$20.4^{+7.2}_{-4.6}$	–	2.7 ± 0.3
Gem OB1	$10.9^{+1.4}_{-2.4}$	–	$2.5^{+0.1}_{-0.6}$
Car OB1	$9.9^{+1.6}_{-1.2}$	–	$3.4^{+0.6}_{-0.8}$
Sco OB1	$4.8^{+0.8}_{-0.6}$	$8.0^{+2.5}_{-1.9}$	2.1 ± 1.4

Our estimates of the kinematic ages of OB associations, T^*, obtained by the second method are smaller than 5 Myr in the Sgr OB1, Gem OB1, Ori OB1, Car OB1, and Sco OB1 associations, which agrees with the following star formation scenario: first OB stars form inside a giant molecular cloud and only then a group of these stars starts its expansion. In the case of the Per OB1, the value of $T^* = 10.6^{+2.6}_{-3.9}$ is only marginally consistent with this sequence of events. Possibly, the Per OB1 association started its expansion with a larger velocity than its present-day value, resulting in a smaller kinematic age (see also Section 3.5).

3.5 Shell-like structure in the distribution of stars in the Per OB1 association

The distribution of stars in two large expanding OB associations, Per OB1 and Car OB1, suggests the presence of a shell-like structure with a density maximum located between the central part and periphery (Fig. 2). To check this hypothesis, we consider the variations of the surface density of OB stars, Σ, with the distance, d, from the centre of the association (Fig. 7a). We subdivided the distribution of stars in the sky plane inside the association into 6-pc wide annuli of radius d with the centres coincident with the centre of the association. The average surface density of stars at the distance d from the centre is the ratio $\Sigma = N/S$, where N is the number of stars in the annulus and S is its area.

Fig. 7(a) shows the presence of a secondary maximum on the curve $\Sigma(d)$ for the Per OB1 association located at the distance of 40 pc from its centre. The secondary maximum is due to the presence of a minimum on the density curve between the central concentration and the periphery. The statistical significance of the secondary maximum is determined by the errors due to Poisson noise in the maximum and minimum density distribution, σ_1 and σ_2, respectively:

$$S = \frac{\Sigma_{\max} - \Sigma_{\min}}{\sigma_1 + \sigma_2}, \tag{31}$$

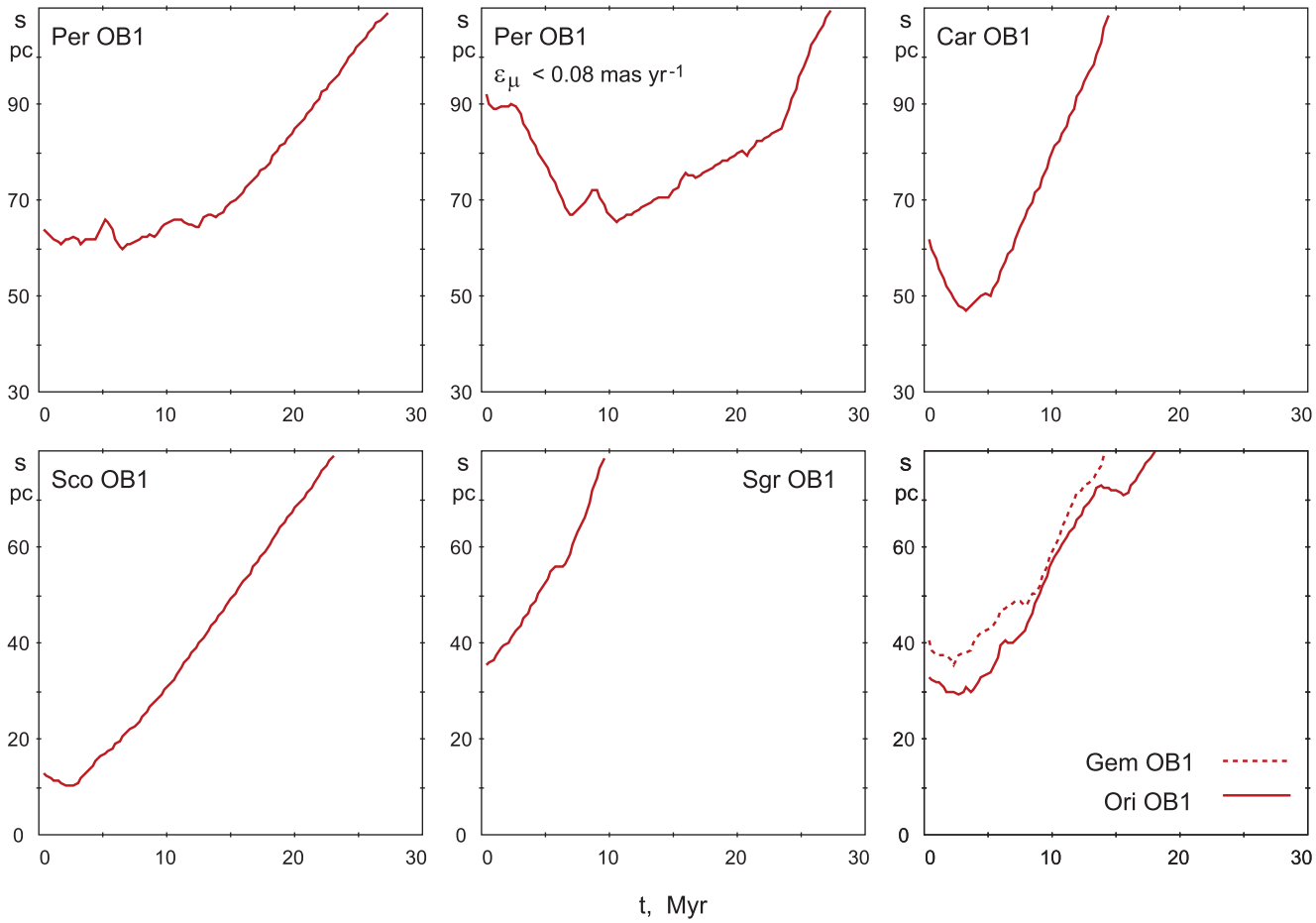

Figure 6. Dependence of the size s of OB association on the time t in the past. Here s is the radius of association containing central 68 per cent of its star members with known *Gaia* DR2 proper motions. In the case of the Per OB1 association, we also show separate plot for the sample of stars with the most precise proper motions ($\varepsilon_{\mu l} < 0.008$ mas yr^{-1} and $\varepsilon_{\mu b} < 0.008$ mas yr^{-1}). Only cases with well-defined parameters of expansion are considered.

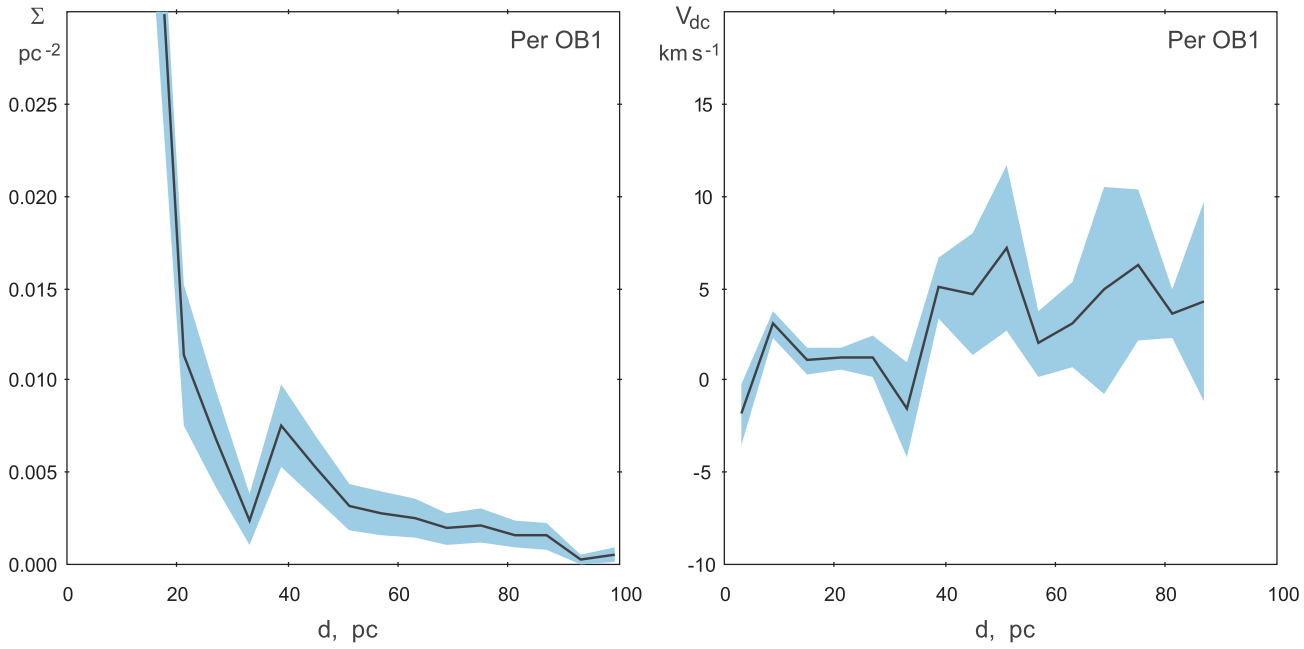

Figure 7. (a) Distribution of OB stars inside the Per OB1 association averaged in thin annuli. The distribution of stars in the sky plane was divided into 6-pc wide annuli of radius d with the centres coincident with the centre of the association. The horizontal and vertical axes measure the distance from the centre, d, and the surface density of stars, Σ, respectively. The uncertainties due to Poisson noise are shown in grey (coloured blue in the online article). We can see the existence of a secondary maximum at the distance of 40 pc from the centre of the association. (b) Dependence of the velocity of expansion, $V_{\rm dc}$, averaged in thin annuli on the distance d. The velocity $V_{\rm dc}$ is the relative corrected velocity in the direction connecting the centre of the association with the star. The velocity of expansion at the distance of the secondary maximum appears to be 5.0 ± 1.7 km s^{-1}. The scatter due to root-mean-square errors in determination of average velocities in each annulus is shown in grey (coloured blue in the online article).

which gives the significance level of $P \sim 1.4\sigma$. We find a similar shell-like structure in the Car OB1 association but it has lower statistical significance and we do not consider it here.

To understand the nature of the secondary maximum, we build the distribution of velocities inside the association. Fig. 7(b) shows the variation of the average expansion velocity, $V_{\rm dc}$, of OB stars with the distance, d, from the centre of the association. The velocity $V_{\rm dc}$ of a star is the component of its relative corrected velocity, (V'_{lc}, V'_{bc}) (equations 18 and 19), directed along the radius–vector, $\overrightarrow{d}$, connecting the centre of the association with the star in the sky plane. We can see that the velocity $V_{\rm dc}$ at the distance of the shell, $d = 40$ pc, amounts to the value of $V_{\rm dc} = 5.0 \pm 1.7$ km s^{-1}. Thus, we can speak about the expanding shell of stars here.

There are two different scenarios of the formation of expanding OB associations. The first one considers the expansion of young stellar group caused by the gas loss in its parent molecular cloud (Hills 1980; Kroupa et al. 2001; Boily & Kroupa 2003a, b; Vine & Bonnell 2003). The second scenario includes two episodes of star formation: the first generation of massive stars creates an expanding gas shell while the second generation of stars, which we observe now, forms from the molecular gas collected by the expanding shell. The radii of the shells are supposed to be 30–150 pc and the velocity of expansion $V_{\rm sh}$ must be less than $V_{\rm sh} < 15$ km s^{-1} (Castor, McCray & Weaver 1975; Elmegreen & Lada 1977; Weaver et al. 1977; Lozinskaya & Sitnik 1988; Lozinskaya 1999, and others). There is a difference between the formation of OB stars in an expanding shell, when stars acquire the expansion velocity at the time of their birth, and the expansion of OB association due to the gas loss in the parent molecular cloud, when stars are born in the turbulent but unexpanding gas medium and begin their motion outwards due to a sudden lack of gravitational force in the centre of the group.

The formation of the Per OB1 association from the molecular gas accumulated by the shell seems to be unlikely. There are two arguments against this scenario. First, we do not observe any difference in ages of OB stars located in the central part and in the expanding shell in the Per OB1 association (Fig. 2). Secondly, the symmetry in the distribution of stars with respect to the centre of the association. If stars were born in an expanding shell, then they would have been formed in gravitationally isolated segments of the shell, which must have a bit different density, so the formation of massive stars throughout the shell in a small time interval looks questionable.

We suppose that the expansion of the Per OB1 association is caused by the gas loss in its parent molecular cloud due to thermal pressure of H II regions. The average radius and expansion velocity of the shell are $d = 40$ pc and $V_{\rm dc} = 5.0 \pm 1.7$ km s^{-1}, respectively. It means that the Per OB1 association started its expansion $T = 8^{+4}_{-2}$ Myr ago. However, the existence of massive O-type stars in the expanding shell, whose ages do not exceed 5 Myr (Fig. 2), suggests that the expansion of the Per OB1 association must have started with a larger expanding velocity and its kinematical age must be smaller than 5 Myr.

Note that the age of the double stellar cluster h and χ Persei located in the centre of the Per OB1 association is supposed to be 10–13 Myr (Dias et al. 2002; Slesnick, Hillenbrand & Massey 2002), which suggests that the formation of their stars could have started 5–8 Myr before the formation of present-day O stars in the Per OB1 association. Probably, stars of the clusters h and χ Persei formed during the time interval when the parent molecular cloud was compressing due to its own gravity but the mean gas density had

not reached its maximal value yet. Simulations show that during the global collapse of the cloud, the average Jeans mass is decreasing and the fraction of gas mass involved in the instantaneous star formation is increasing, so the initial mass function is expected to be sufficiently sampled to produce massive stars, which then begin to erode the cloud (Zamora-Aviles, Vazquez-Semadeni & Colin 2012; Colin et al. 2013, Dale, Ercolano & Bonnell 2012). Probably, the giant molecular cloud in which the Per OB1 association formed had very dense central part that allowed it to produce a lot of massive stars during a small time interval.

4 DISCUSSION AND CONCLUSIONS

We studied the velocities in the sky plane, v_l and v_b, inside 28 OB associations including more than 20 *Gaia* DR2 stars. The average velocity dispersion inside 28 associations is $\overline{\sigma_v} = 4.5 \pm 0.3$ km s^{-1}, which exceeds the corresponding value derived from *Gaia* DR1 proper motions, $\overline{\sigma_v} = 3.5 \pm 0.5$ km s^{-1}, at the significance level of $P \sim 1\sigma$. The greater value of σ_v obtained with *Gaia* DR2 proper motions can be both due to statistical effects and due to shorter time baseline, which makes the results more sensitive to all sorts of systematic effects.

Kounkel et al. (2018) found that the line-of-sight velocities of stars inside the Ori OB1 association obtained with the uncertainty less than 1 km s^{-1} and corrected for the motion of the Sun towards the standard apex lie in the range of 0–15 km s^{-1}, which is consistent with the velocity dispersion of 3–5 km s^{-1}.

We used the velocity dispersion σ_v inside OB associations and their radii a to calculate the virial masses of OB associations, which are equal to the masses of their parent giant molecular clouds. The median virial mass computed for 28 OB associations is $M_{\rm vir} = 8.9 \times 10^5$ M$_\odot$. We also determined the stellar masses of OB associations. Here we used the power law distribution of stars over masses by Kroupa (2002) calibrated through the number of massive stars in OB association. The median stellar mass of OB associations is $M_{\rm st} = 8.1 \times 10^3$ M$_\odot$. The stellar-to-virial mass ratio determines the average star formation efficiency inside the giant molecular cloud, which has the median value of $\epsilon = 1.2$ per cent.

We found that the Sgr OB1, Per OB1, Ori OB1, Gem OB1, Car OB1, and Sco OB1 associations are expanding at a significance level of $P > 3\sigma$. The expansion of the Per OB1, Car OB1, and Sgr OB1 associations first has been found with *Gaia* DR1 proper motions (Melnik & Dambis 2017). *Gaia* DR2 data confirm their expansion and suggest three new expanding associations: Ori OB1, Gem OB1, and Sco OB1. The Ori OB1 association shows expansion only after the correction of velocities v_l and v_b for the line-of-sight motion of the association as a whole; it also displays the expansion along the line of sight. The expansion of the Gem OB1 association was found only after the exclusion of five stars with the error RUWE $>$ 1.4 from consideration. Only two associations (Per OB1 and Sco OB1) show well-defined expansion in both the l and b directions, the other associations demonstrate expansion at a significance level of $P > 3\sigma$ in one direction only.

We gave evidence in favour of the expanding stellar shell in the Per OB1 association with the radius of $d = 40$ pc and the expansion velocity of $V_{\rm dc} = 5.0 \pm 1.7$ km s^{-1}, which suggests that the expansion of OB stars started $T = 8^{+4}_{-2}$ Myr ago. However, the existence of massive O-type stars in the expanding shell with the ages less than 5 Myr suggests that the expansion of the Per OB1 association started with a larger expanding velocity, resulting in a smaller kinematic age.

We can see that the expansion of OB associations is quite a rare event: it is observed only in six from 28 associations considered, i.e. the frequency of this event is ∼21 per cent. There are two possible reasons of such a low frequency of expanding OB associations. First, it is the lack of precise proper motions for stars of OB associations, so the expansion is merely washed out by noise. Secondly, it is a physical reason – only the most dense giant molecular clouds can produce stellar groups expanding from one centre, while less dense clouds produce several groups inside one cloud each of which is expanding from its centre, so the total velocity distribution looks chaotic.

We found a strong correlation between the re-normalized unit weight errors (RUWE) and the relative velocities (equations 16 and 17) of member stars determined with respect to the centre of OB association. Note that among 33 stars moving with the relative velocities more than 50 km s^{-1}, the fraction of stars with RUWE $>$ 1.4 amounts to 48 per cent but the expected fraction is only 9 per cent.

ACKNOWLEDGEMENTS

We thank the anonymous referee for fruitful discussion. This work has made use of data from the European Space Agency (ESA) mission *Gaia* (https://www.cosmos.esa.int/gaia), processed by the *Gaia* Data Processing and Analysis Consortium (DPAC, https://www.cosmos.esa.int/web/gaia/dpac/consortium). Funding for the DPAC has been provided by national institutions, in particular, the institutions participating in the *Gaia* Multilateral Agreement. This research has made use of the VizieR catalogue access tool, CDS, Strasbourg, France. The original description of the VizieR service was published by Ochsenbein, Bauer & Marcout (2000). A.K. acknowledges the support from the Russian Foundation for Basic Research (project nos. 18-02-00890 and 19-02-00611).

REFERENCES

Ambartsumian V. A., 1949, Soviet Astron. Zhurn., 26, 3
Arenou F. et al., 2018, A&A, 616, 17
Barbier-Brossat M., Figon P., 2000, A&AS, 142, 217
Baumgardt H., Kroupa P., 2007, MNRAS, 380, 1589
Blaauw A., 1964, ARA&A, 2, 213
Blaha C., Humphreys R. M., 1989, AJ, 98, 1598
Boily C. M., Kroupa P., 2003a, MNRAS, 338, 665
Boily C. M., Kroupa P., 2003b, MNRAS, 338, 673
Bressan A., Marigo P., Girardi L., Salasnich B., Dal Cero C., Rubele S., Nanni A., 2012, MNRAS, 427, 127
Brown A. G. A., Dekker G., de Zeeuw P. T., 1997, MNRAS, 285, 479
Brown A. G. A. et al., 2018, A&A, 616, A1
Cantat-Gaudin T. et al., 2019, A&A, 626, 17
Castor J., McCray R., Weaver R., 1975, ApJ, 200, L107
Chen H.-R. et al., 2019, ApJ, 875, 24
Colín P., Vázquez-Semadeni E., Gómez G. C., 2013, MNRAS, 435, 1701
Dale J. E., Ercolano B., Bonnell I. A., 2012, MNRAS, 427, 2852
Dambis A. K., Melnik A. M., Rastorguev A. S., 2001, Astron. Lett., 27, 58
Dias W. S., Alessi B. S., Moitinho A., Lépine J. R. D., 2002, A&A, 389, 871
Elmegreen B. G., 1983, MNRAS, 203, 1011
Elmegreen B. G., Lada C. J., 1977, ApJ, 214, 725
ESA, 1997, The HIPPARCOS and TYCHO Catalogues. Astrometric and Photometric Star Catalogues Derived from the ESA HIPPARCOS Space Astrometry Mission, ESA SP- 1200
Evans N. J. et al., 2009, ApJS, 181, 321
Franco J., Shore S. N., Tenorio-Tagle G., 1994, ApJ, 436, 795
Fujii M. S., Portegies Zwart S., 2011, Science, 334, 1380

Gaia Collaboration, 2016, A&A, 595, A1
Garcia P., Bronfman L., Nyman L.-A., Dame T. M., Luna A., 2014, ApJS, 212, 2
Hills J. G., 1980, ApJ, 225, 986
Jordi C. et al., 2010, A&A, 523, A48
Katz D. et al., 2018, A&A, 616, A11
Kauffmann J., Pillai Th., Goldsmith P., 2013, ApJ, 779, 185
Kim J.-G., Kim W.-T., Ostriker E. C., 2016, ApJ, 819, 137
Kounkel M. et al., 2018, AJ, 156, 84
Kroupa P., 2002, Science, 295, 82
Kroupa P., Aarseth S., Hurley J., 2001, MNRAS, 321, 699
Krumholz M. R., Matzner C. D., McKee C. F., 2006, ApJ, 653, 361
Larson R. B., 1981, MNRAS, 194, 809
Lindegren L., 2018, Gaia technical note GAIA-C3-TN-LU-LL-124. https://www.cosmos.esa.int/web/gaia/ll-124
Lindegren L., 2019, A&A, 633, A1,
Lindegren L. et al., 2016, A&A, 595, A4
Lindegren L. et al., 2018, A&A, 616, A2
Lozinskaya T. A., 1999, ASP Conf. Ser., 168, 427
Lozinskaya T. A., Sitnik T., 1988, Sov. Astron. Lett., 14, 100
Madsen S., Dravins D., Lindegren L., 2002, A&A, 381, 446
McKee C. F., 1989, ApJ, 345, 782
Melnik A. M., 2019, MNRAS, 485, 2106
Melnik A. M., Dambis A. K., 2009, MNRAS, 400, 518
Melnik A. M., Dambis A. K., 2017, MNRAS, 472, 3887
Melnik A. M., Dambis A. K., 2018, Astron. Rep., 62, 997
Melnik A. M., Efremov Yu. N., 1995, Astron. Lett., 21, 10
Michalik D., Lindegren L., Hobbs D., 2015, A&A, 574, 115
Myers P. C., Dame T. M., Thaddeus P., Cohen R. S., Silverberg R. F., Dwek E., Hauser M. G., 1986, ApJ, 301, 398
Ochsenbein F., Bauer P., Marcout J., 2000, A&AS, 143, 23
Pecaut M. J., Mamajek E. E., 2016, MNRAS, 461, 794
Riess A. G. et al., 2018, ApJ, 861, 126
Sanders D. B, Scoville N. Z., Solomon P. M., 1985, ApJ, 289, 373
Sitnik T. G., Melnik A. M., 1996, Astron. Lett., 22, 422
Slesnick C. L., Hillenbrand L. A., Massey P., 2002, ApJ, 576, 880
Stassun K. G., Torres G., 2018, ApJ, 862, 61
Vine S. G., Bonnell I. A., 2003, MNRAS, 342, 314
Ward J. L., Kruijssen J. M. D., 2018, MNRAS, 475, 5659
Weaver R., McCray R., Castor J., Shapiro P., Moore R., 1977, ApJ, 218, 377
Wright N. J., Mamajek E. E., 2018, MNRAS, 476, 381
Yalyalieva L. N., Chemel A. A., Glushkova E. V., Dambis A. K., Klinichev A. D., 2018, Astrophys. Bull., 73, 335
Zamora-Aviles M., Vazquez-Semadeni E., Colin P., 2012, ApJ, 751, 77
Zinnecker H., Yorke H. W., 2007, ARA&A, 45, 481

SUPPORTING INFORMATION

Supplementary data are available at *MNRAS* online.

Table 1.

Please note: Oxford University Press is not responsible for the content or functionality of any supporting materials supplied by the authors. Any queries (other than missing material) should be directed to the corresponding author for the article.

APPENDIX A.

Here is the list of 17 stars of OB associations with the absolute values of the relative velocities, V_l' or V_b', greater than 50 km s^{-1}, which were excluded from our consideration in the study of the expansion of OB associations (Section 3.3): HD 163065 (Sgr OB5), HD 166937A (Sgr OB1), HD 172488 (Sct OB2), HD 192445 (Cyg OB3), HD 192281 (Cyg OB8), HD 212043 (Cep OB2), HDE 240331 (Cas OB2), BD +59 70 (Cas OB4), BD +62 68 (Cas OB4), HILTNER 74 (Cas OB7), BD + 60 261 (Cas OB8), HD 12323 (Per OB1), BD + 60 512 (Cas OB6), HD 73634 (Vela OB1), HD 94024 (Car OB1), HD 102248 (Cru OB1), and HD 112272 (Cen OB1).

This paper has been typeset from a TEX/LATEX file prepared by the author.